chemosensors

Article

First Direct Gravimetric Detection of Perfluorooctane Sulfonic Acid (PFOS) Water Contaminants, Combination with Electrical Measurements on the Same Device—Proof of Concepts

George R. Ivanov [1,*], Tony Venelinov [2], Yordan G. Marinov [3], Georgi B. Hadjichristov [3], Andreas Terfort [4], Melinda David [5,6], Monica Florescu [6] and Selcan Karakuş [7]

1 University Laboratory "Nanoscience and Nanotechnology", University of Architecture, Civil Engineering and Geodesy, 1 Hr. Smirnenki blvd., 1064 Sofia, Bulgaria
2 Laboratory for Water Analysis, University of Architecture, Civil Engineering and Geodesy, 1 Hr. Smirnenki blvd., 1064 Sofia, Bulgaria; tvenelinov_fhe@uacg.bg
3 Institute of Solid State Physics, Bulgarian Academy of Sciences, 72 Tzarigradsko Chaussee blvd., 1784 Sofia, Bulgaria; ymarinov@issp.bas.bg (Y.G.M.); georgibh@issp.bas.bg (G.B.H.)
4 Department of Chemistry, Institute of Inorganic and Analytical Chemistry, Goethe University Frankfurt, Max-von-Laue-Str. 7, 60438 Frankfurt, Germany; aterfort@chemie.uni-frankfurt.de
5 Laboratory for Quality Control and Process Monitoring, University of Bucharest, 4-12 Elisabeta Blvd., 030018 Bucharest, Romania; melinda.david@s.unibuc.ro
6 Department of Fundamental, Prophylactic and Clinical Disciplines, Transilvania University of Braşov, Str. Universitatii No. 1, 500068 Brasov, Romania; florescum@unitbv.ro
7 Department of Chemistry, Faculty of Engineering, Istanbul University-Cerrahpaşa, 34320 Istanbul, Turkey; selcan@iuc.edu.tr
* Correspondence: george@at-equipment.com; Tel.: +359-885-465-535

Abstract: Perfluoroalkyl and polyfluoroalkyl substances (PFAS) are pollutants of concern due to their long-term persistence in the environment and human health effects. Among them, perfluorooctane sulfonic acid (PFOS) is very ubiquitous and dangerous for health. Currently, the detection levels required by the legislation can be achieved only with expensive laboratory equipment. Hence, there is a need for portable, in-field, and possibly real-time detection. Optical and electrochemical transduction mechanisms are mainly used for the chemical sensors. Here, we report the first gravimetric detection of small-sized molecules like PFOS (MW 500) dissolved in water. A 100 MHz quartz crystal microbalance (QCM) measured at the third harmonic and an even more sensitive 434 MHz two-port surface acoustic wave (SAW) resonator with gold electrodes were used as transducers. The PFOS selective sensing layer was prepared from the metal organic framework (MOF) MIL-101(Cr). Its nano-sized thickness and structure were optimized using the discreet Langmuir–Blodgett (LB) film deposition method. This is the first time that LB multilayers from bulk MOFs have been prepared. The measured frequency downshifts of around 220 kHz per 1 µmol/L of PFOS, a SAW resonator-loaded Q_L-factor above 2000, and reaction times in the minutes' range are highly promising for an in-field sensor reaching the water safety directives. Additionally, we use the micrometer-sized interdigitated electrodes of the SAW resonator to strongly enhance the electrochemical impedance spectroscopy (EIS) of the PFOS contamination. Thus, for the first time, we combine the ultra-sensitive gravimetry of small molecules in a water environment with electrical measurements on a single device. This combination provides additional sensor selectivity. Control tests against a bare resonator and two similar compounds prove the concept's viability. All measurements were performed with pocket-sized tablet-powered devices, thus making the system highly portable and field-deployable. While here we focus on one of the emerging water contaminants, this concept with a different selective coating can be used for other new contaminants.

Keywords: gravimetry; perfluoroalkyl and polyfluoroalkyl substances (PFAS); PFOS; metal-organic frameworks (MOF); MIL-101(Cr); surface acoustic wave (SAW) resonators; quartz crystal microbalance (QCM); Langmuir–Blodgett (LB) films; chemical sensors; water purity monitoring; electrochemical impedance spectroscopy (EIS)

check for updates

Citation: Ivanov, G.R.; Venelinov, T.; Marinov, Y.G.; Hadjichristov, G.B.; Terfort, A.; David, M.; Florescu, M.; Karakuş, S. First Direct Gravimetric Detection of Perfluorooctane Sulfonic Acid (PFOS) Water Contaminants, Combination with Electrical Measurements on the Same Device—Proof of Concepts. *Chemosensors* **2024**, *12*, 116. https://doi.org/10.3390/chemosensors12070116

Received: 19 April 2024
Revised: 14 June 2024
Accepted: 18 June 2024
Published: 22 June 2024

1. Introduction

"Per- and polyfluorinated alkyl substances" (PFAS) is used as a generic term for highly fluorinated aliphatic substances consisting of at least one fully fluorinated carbon atom ($–CF_2$) [1]. The C–F chemical bond is very strong, which makes these chemicals very stable and highly resistant to hydrolysis, metabolism, photolysis, and other forms of degradation [2]. The adverse effects on human health have made these emerging contaminants part of the legislation protecting the environment and humans worldwide. For example, in the latest European Union Directive on the water intended for human consumption [3], the maximum allowable level of PFAS contaminants in water was set to 0.1 µg/L, and 20 PFAS substances with $–C_nF_{2n}–$ chains between 3 and 13 carbon atoms were identified as the most dangerous and subject to control. The updated advisory levels, which are based on new science and consider lifetime exposure, indicate that some adverse health effects may occur with concentrations of perfluorooctanoic acid (PFOA) or perfluorooctane sulfonic acid (PFOS) in water that are near zero according to the US Environmental Protection Agency (EPA) [4]. This is one reason that this research focuses on the PFOS compound [5].

To measure the low levels of these contaminants, enrichment with solid-phase extraction is required, followed by chromatographic techniques combined with mass spectroscopy [1,6]. These methods are very sensitive and precise, but their use has many drawbacks. They require expensive laboratory instrumentation, well-trained personnel, and extra care in sampling to avoid contamination, and there is a significant time lag between taking the sample and producing results. Hence, there is a considerable demand for in-field sensors that can continuously monitor water purity for PFAS contaminants in real time. Several groups are working toward this goal, and their work has been reviewed recently [1,5–7].

A fast chemical sensor requires special attention in preparing a thin, uniform, and well-controlled sensing layer. Compared to simple deposition techniques like spin coating, dip casting, and sputtering, the Langmuir–Blodgett (LB) discreet layer deposition method is considered much superior [8,9]. The LB technique can be used with a wide variety of compounds, including organic molecules, nanoparticles, enzymes, and nanocomposites. This fabrication technique is favorable for practical application as it allows fine control over film thickness, uniformity, and molecular orientation and can be combined with surface functionalization. Still, it is one of the most complex nano-thin layer technologies and requires expensive equipment [9]. In some cases, layer-by-layer (LbL) and self-assembled monolayers (SAMs) can also provide suitable coating characteristics [8].

The sensing layer has to be selective to the PFAS contaminants. Here, the choices are limited to only a few options. Molecularly imprinted polymers (MIPs) can provide sufficient selectivity [7,10,11]. While MIPs are chemically and physically more stable than natural receptors, there are still problems with incomplete template extraction, or the binding sites can interact with more than one analyte, affecting sensor reproducibility. The first and only aptamer-based PFAS sensor was recently produced by a self-developed aptamer [12]. However, aptamers are less physically and chemically stable toward the in-field environment and can degrade enzymatically [7]. A third alternative for the PFAS sensing layer is the metal-organic frameworks (MOFs). These are crystalline hybrid materials consisting of transition metal ions coordinated to organic molecules, forming a well-structured periodic 3D framework architecture. These advanced materials can be compared with sponges. Due to their versatile porous structure, high surface area, and chemical and thermal stability [13], MOFs show unique abilities—taking up, holding, and releasing molecules from their pores by applying different stimuli such as heat, pressure, light, or a magnetic field. They are deemed suitable for various applications, such as gas storage and separation, catalysis, energy conversion, and biomolecule encapsulation [14]. Their fabrication, modification, and patterning progress is constantly monitored [15–17].

MOF nanosheets created using the LB method are a promising field of supramolecular architecture design [18]. For such applications, the MOF crystals' different sizes,

morphologies, and orientations are studied using XRD and SEM [19]. MOF nanofilms (such as NAFS) are obtained using LB and LbL [20,21]. Alternatively, ultrathin MOF and polymer films of NH_2-MIL88B(Fe) and a commercial polyimide were produced using the LB method [22]. Such films are successfully used to obtain ultrathin MOF-based mixed matrix membranes [23]. The preparation of MOF thin films also from bulk crystals is reviewed in [24]. A greener method was proposed to synthesize MIL-101(Cr) and prepare some 100 nm-thick films using dip-coating [25]. The only LB films of MOF nanoparticles, only three LB layers thick, were tested for CO_2 absorption by QCM [26]. $Cr_3F(H_2O)_2O$[benzenedicarboxylate]$_3$.nH_2O (MIL-101(Cr)) MOF was shown to be very effective in CO_2 adsorption [26], the detection of VOCs [27–30], bisphenol A [31], formaldehyde [32], pigments [33], humidity [34], gas sensing [35], and tumor marker detection [36].

The MOF MIL-101(Cr) is chosen in this study as it is very efficient at PFOS adsorption and removal [37]. It was shown that MIL-101(Cr) can adsorb significantly more PFAS compared to zeolites, activated carbon, and other porous structures and MOFs [38]. It is stable in water, commercially available from reputable sources, and very selective and sensitive to the PFOS contaminant tested here [39]. Its selectivity was proven even when given the challenge of tackling groundwater. Using this MOF, the highest sensitivity in situ sensor for the PFOS contaminants was realized using electrical impedance detection [39]. Our work, for the first time, makes a preliminary investigation, optimization, and deposition of LB films from bulk MOFs and thus creates superior and faster sensing layers.

The gravimetric transduction mechanism is considered the best method in sensor transduction because there is no need for data interpretation—the adsorbed mass is directly related to the measured analyte concentration. Gravimetric acoustic devices like SAW resonators and QCMs were readily used for measurements in the gas phase or detecting heavy biological molecules or whole cells in liquids [40–42]. So far, no PFAS or similar small molecule detection has been made with a gravimetric device in liquid media. Here, we present a proof of concept that this is possible. The results from the most sensitive acoustic resonators QCM at 100 MHz resonant frequency measured in the first and third harmonics in water showed no monotone change in the resonant frequency downshift on PFOS concentration increase. However, an even more sensitive two-port SAW resonator at 434 MHz tested in the air after analyte adsorption from water showed an almost linear frequency downshift at micromolar PFOS concentrations. This was combined with electrochemical impedance spectroscopy (EIS) measurements using the strong signal-enhancing effect of the SAW resonator's interdigitated microelectrode structure. [39]. Thus, additional sensor selectivity is achieved, as the different transduction methods on a single device can differentiate between two analytes with similar responses in one method but different in the other.

2. Materials and Methods

2.1. Materials

The MOF MIL-101(Cr) was purchased in powder form from NovoMOF AG (Zofingen, Switzerland). The nitrogen adsorption-desorption tests (Figure S1) yielded a surface area of 3269.3 m^2/g, which is above the average for this material and shows minimal hysteresis. The material X-ray diffraction pattern (Figure S2) corresponds to the previously published XRD experimental and calculated data [43]. The peak sharpness indicates the well-ordered crystalline structure of the MOF crystals. The scanning electron microscopy (SEM) data (Figure 1) show significant substance agglomeration. Aggregates in the range of 5 to 50 µm can be seen. The large aggregation can be due to the long storage of the material before its use (years) or to the synthesis method used. Individual MIL-101(Cr) crystals are observed on further magnification ranging from 220 nm to 450 nm. The arachidic acid (AA—$CH_3(CH_2)_{18}COOH$) used was with 98% purity (Alfa Aesar, Karlsruhe, Germany). Perfluorooctanesulfonic acid, $CF_3(CF_2)_7SO_3H$ (PFOS) analytical standard in approximately 40% water, sodium dodecyl sulfate $CH_3(CH_2)_{11}OSO_3Na$ (SDS) with a purity of >99%, and perfluorooctanoic acid $CF_3(CF_2)_6COOH$ (PFOA) with a purity of >99.5% were purchased

from Merck (Darmstadt, Germany). All solvents used were of pro analysis purity. For EIS measurements, a 0.1 M pH 7.4 PB buffer was prepared.

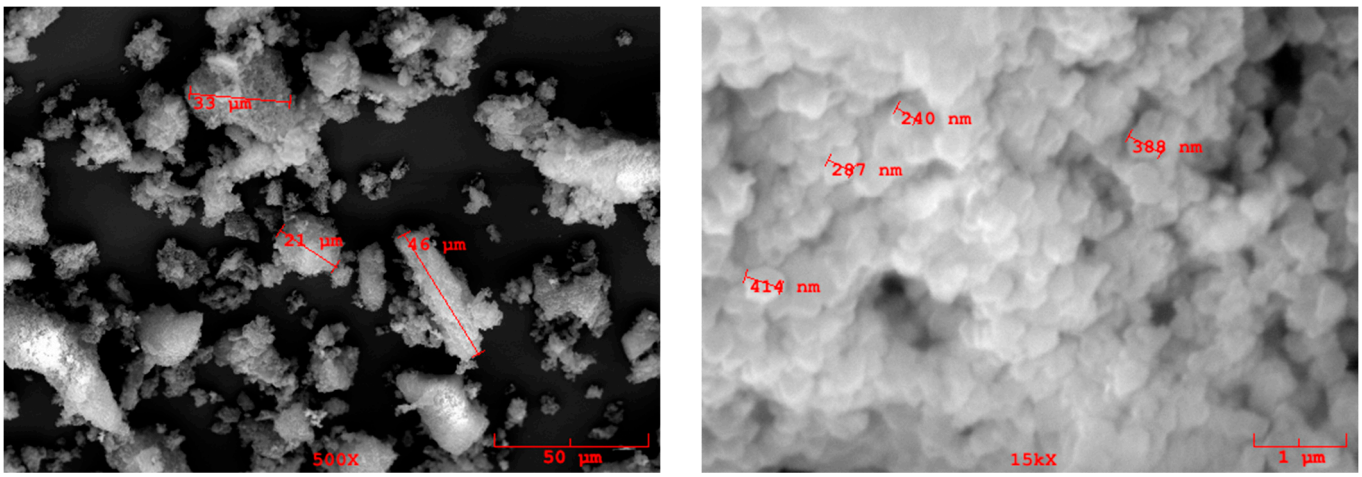

(**a**) (**b**)

Figure 1. SEM images at a 50 µm scale (**a**) and 1 µm scale (**b**) of as-received MOF MIL-101(Cr). Significant substance aggregation can be seen.

The water used both for the subphase in the LB film preparation and for immersing the SAW resonators in the PFOS solutions was filtered with a set of 3 reverse osmosis filters, 4 activated carbon filters, an ion exchange filter (Boeco, Hamburg, Germany), and a final 0.1 µm pore filter. Its conductivity measured during these experiments was 1.45 µS/cm, much higher than the 0.055 value for ultra-pure water. However, testing the water with an atom emission spectrometer with inductively coupled plasma mass spectrometry did not show the presence of any metal ions above the limit of determination of the instrument (ng/L).

2.2. MOF Dispersion Preparation

To prepare the spreading dispersion for the Langmuir films, 100 mg of MIL-101(Cr) powder was dispersed in a solvent mixture of 20% by volume of methanol and 80% chloroform. The chloroform immiscibility with water keeps the droplets of the dispersion afloat at the air–water interface on Langmuir film preparation, allowing for excellent spread and minimum loss of substance into the water volume. At the same time, the methanol will improve the polar moieties dispersion. A dispersion with a concentration of 20 mg/mL was obtained. The homogenization was carried out at room temperature (23 °C) using ultrasonic treatment at 20 kHz, 1200 W lab sonicator (Hangzhou Dowell Ultrasonic Tech Co., Ltd., Hangzhou, China). The ultrasound mixer was operated at 600 W for 60 min. In some cases, the dispersion was subsequently filtered through 0.45 µm and 0.2 µm pore PTFE syringe filters. Afterward, the stock dispersion was diluted with the same solvents to a 1 mg/mL concentration. Langmuir and LB films were prepared from pure MOF or with added AA lipid to 3% by mass to improve film homogeneity. In [26], a bit longer fatty acid (Behenic acid) with 1% by mass was shown to improve the LB film homogeneity. However, small pinholes were still observed, which is especially problematic in electrical measurements. So, we increased the amount of fatty acid added to minimize these pinhole defects. Before each spread of the MOF solution, it was sonicated for 1 h in a standard ultrasound sonicator.

2.3. The SAW Resonators Used

Specially developed and optimized for chemical sensor applications Rayleigh-type 434 MHz SAW two-port resonators with gold electrodes were used in the present study. Unlike QCMs, they can not be used in liquid media. Still, they have around 4200 times higher relative, independent of device frequency, mass sensitivity and a 3000 times lower

limit of detection (LOD) compared to a 5 MHz QCM and are much better suited for applications in which the QCM does not provide sufficient sensitivity [44]. Other advantages are their low insertion loss (less than 8 dB, including the connectors), excellent thermal stability, and very high loaded Q-factor, which is very important in obtaining a low LOD. As shown in [45], when connected to a sensor oscillator circuit, such a resonator can have short-term stability of a few parts in 10^{-10} Hz, providing LOD levels in the pg and even fg range [46]. The loaded Q_L of the device was calculated from its narrowband group delay reading τ_g, measured with the VNA using the formula $Q_L = \pi f_o \tau_g$. With a typical τ_g = 2.1 µs at the resonance frequency f_o = 434.2 MHz, the SAW resonators used in this study have an initial Q_L-factor of around 2870. This value gradually decreases during LB film deposition and PFOS loading. We have successfully used these resonators for volatile organic compound (VOC) measurements in the gas phase [47]. The protocol for mass calibration is described there, which gives a mass coefficient of M_s = 43.5 kHz/ng. The resonators were bonded in a gold-coated SMD case, and a pair of connectors were soldered.

2.4. LB Film Preparation and PFOS Test Protocol

An LB system model OpenLB® (Advanced Technologies Ltd., Sofia, Bulgaria) was used for the Langmuir film measurements and LB film deposition. The trough was made from a single piece of hydrophobic PTFE, and the symmetrical compression barriers were made of hydrophilic material to avoid film leaks. A fast Wilhelmy-type filter paper surface pressure sensor was used. The open software written in LabView version 2016 allows for displaying both surface pressure as a function of area per mg substance and surface pressure versus time in a rolling 100 s window on a single screen. Detailed control of the constant pressure PID parameters and real-time visualization are on the same screen. The trough was cleaned before experiments with detergent, a brush, and hot water, followed by rinsing with ultra-pure water. A new filter paper was put on the pressure sensor and calibrated against pure water surface tension before each new experiment. The lack of surface-active contaminants in the subphase water was checked by compressing the barriers and monitoring for the surface pressure to be zero before each layer spread. After spreading the layer, it evaporated for at least 40 min before compression. The velocity of compression was 2 cm^2/min. All the substrates for LB film deposition before immersion in the LB system dipping well were cleaned for 2:30 min at 12 W in an air plasma using a plasma cleaner (Harrick Plasma, Ithaca, NY, USA). This cleaning protocol was found to be optimal in providing a clean surface without degrading the electrodes. The air plasma not only gently cleans the surface, unlike the use of heavier atoms (e.g., Ar), but also makes it more hydrophilic, which is essential for quality deposition on the upstroke for the first LB layer. Sometimes, up to 5 h after plasma cleaning of the SAW resonator was needed before a stable mass reading was achieved. Before LB film deposition, the layer was kept at constant pressure for 30 min to allow for stabilization. All isotherms were measured at 22–23 °C. If a second layer on the down stroke was deposited, 20 min were allowed for the first layer to dry, or a complete drying was performed to measure the deposited mass. Flat gold and ultra-flat Si wafers (roughness of around 0.1 nm), also used as substrates, were purchased from NanoAndMore GmbH (Wetzlar, Germany).

The developed test protocol for PFOS testing was the following: After LB film deposition and the complete drying of the SAW resonator, the layer was rinsed at least once in pure water to establish a baseline. A borosilicate glass vessel containing 100 mL of pure water was used in all cases. Afterward, a PFOS solution from a 1 mmol/L stock solution was added with a precision 50 µL syringe. In all instances, magnetic stirring was used. Our measurements with the 100 MHz QCM have shown that 4–5 min are enough for the MOF layer to be saturated with water solution. Also, EIS measurements during immersion in the solution show stabilization of spectra within 20 min. To be safe, every immersion in the water was precisely 46 min. The resonators were handled with a new pair of plastic gloves to eliminate contamination whenever they were wet. The excess water from the SMD case was gently absorbed with filter paper under a magnifying glass. The resonance

was measured and then the resonator was placed in regulated hot (approximately 35 °C) air for 75 min, which was enough for complete drying, confirmed with longer dryings. This temperature is below the tail-melting temperature of AA and is safe for the structure.

2.5. Other Instruments Used

The X-ray photoelectron spectroscopy (XPS) studies were performed in a VG Escalab MKII electron spectrometer using achromatic AlKα radiation with an energy of 1486.6 eV under a base pressure of 10^{-8} Pa and a total instrumental resolution of 1 eV. The binding energies (BE) were determined utilizing the C 1s line as a reference, with an energy of 285.0 eV. The accuracy of the measured BE was 0.2 eV. C1s, O1s, Si2p, Cr2p, and F1s photoelectron lines were recorded. Atomic force microscopy was performed on an Asylum Research (Oxon, UK) MFP-3D Origin instrument in contact mode using soft 2.5 N/m probes. Gravimetry data were measured using a laptop-controlled, pocket-sized vector network analyzer (VNA), PocketVNA (PocketVNA, Rohrdorf, Germany), connected to the samples via semi-rigid coaxial cables. The instrument was calibrated for the measuring range with the supplied accessories. The SAW resonators were measured in a two-port configuration measuring S21. Both magnitude in dB and group delay in μs were displayed. The 100 MHz QCM resonators were in plastic support, and their corresponding E-QCM cell was purchased from Advanced Wave Sensors (AWSensors, Valencia, Spain). The measurement was in reflectivity mode S11, and the peaks were negative. There is an opening in the cell, and 200 μL of buffer was pipetted. PFOS from a 25 μmol/L stock solution was added with a micro syringe. EIS and cyclic voltammetry (CV) measurements were performed with a laptop-operated PalmSens4 instrument (PalmSens BV, Houten, The Netherlands). A −120 mV DC was used in all cases because CV shows a significant difference between pure and PFOS-contaminated buffers in this region. For measurements in the PB buffer, a 20 mV AC was used. In most cases, the scan range was from 1 MHz to 50 mHz, and sometimes scanning to 1 mHz was performed.

3. Results and Discussions

After the MIL-101(Cr) dispersion preparation, it had a green color. Part of it was passed through a 0.2 μm pore PTFE syringe filter, trying to eliminate large aggregates. This resulted in a transparent dispersion, which still formed a monolayer at the air–water interface. To check whether MOF was present in the dispersion, we compared the XPS data of drop-casted dispersions on Si wafers from the green and transparent preparations (Figure 2). The Cr line is missing in the transparent dispersion, indicating that there was no MIL-101(Cr) in it. So, there are no MOF crystals with sizes below 0.2 μm, which can explain the increased roughness of the obtained coatings (see the AFM images below). The Cr2p photoelectron spectra showed that the Cr is in a 3+ state. To confirm the PFOS capture by the MIL-101(Cr) sensing layer, we tested the G60 sample after all the soaking tests described below. The instrument lacked sensitivity and the Cr line was obscured by the strength of the lines from the gold electrodes and the quartz substrate (Figure 2b). We prepared a new sample, Si63, by depositing 1 LB layer from MIL-101(Cr) + AA at a surface pressure of 10 mN/m and 1 h for film stabilization at that pressure, which resulted in more MOF deposited. This sample was soaked overnight in pure water, to which 1.5 μmol/L PFOS was added. We checked the sulfur line to prove the presence of absorbed PFOS (Figure 2e). However, the S2p peak is close to the Si2s peak and, more precisely, is close to the Si plasmon loss peak (17 eV from the main peak). The Si plasmon loss peak was deconvoluted, and the S2p peak could be seen (Figure 2e). This proves the presence of PFOS in the MOF LB monolayer. As described in detail below, the sensor is immersed in ultra-pure water for 46 min, and it adsorbs nothing, as measured gravimetrically. Then, PFOS was added to this water, and the sensor adsorbs something. This something can be only PFOS.

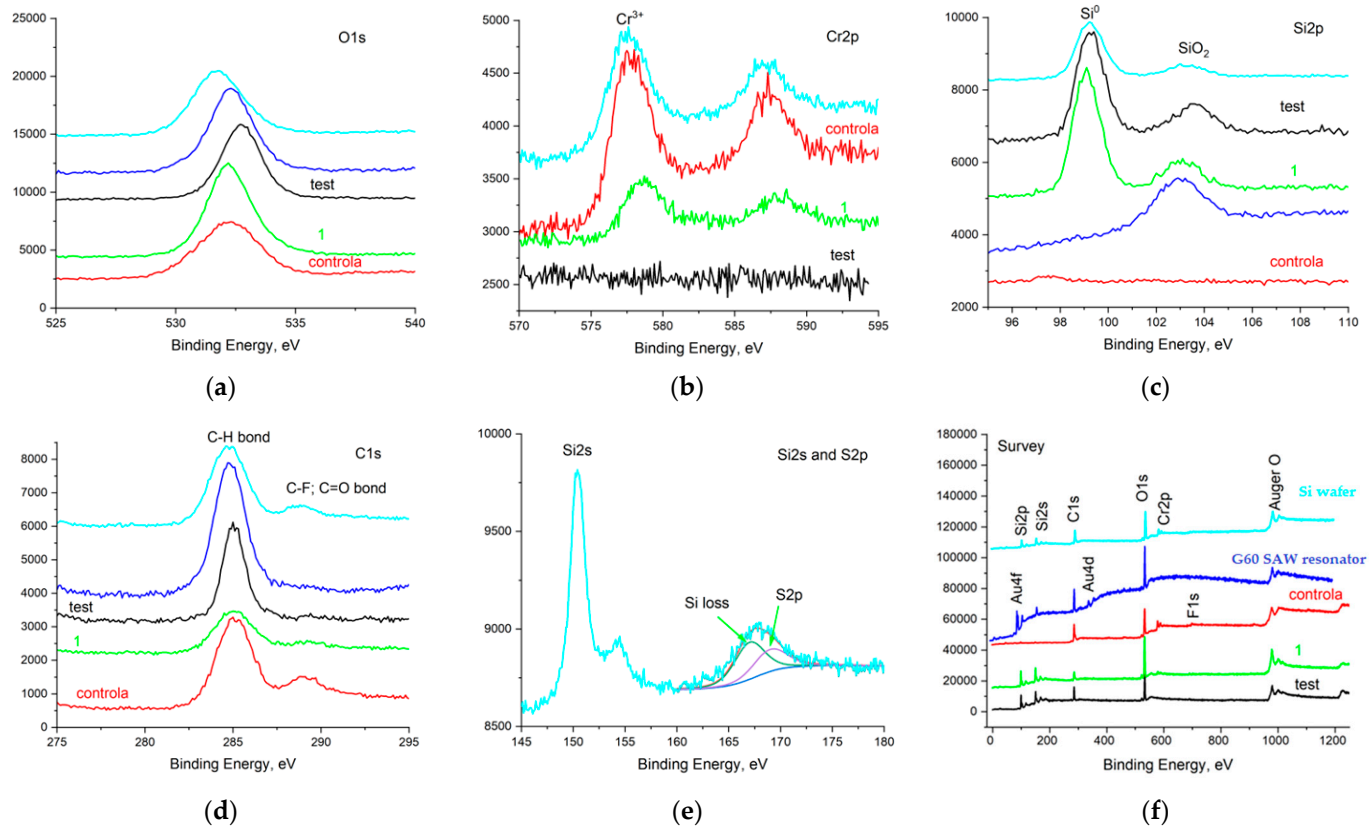

Figure 2. XPS data of drop-casted MIL-101(Cr) dispersions on Si wafer. Black line labeled test—transparent filtered dispersion; red line labeled control—non-filtered with a green color dispersion; green line labeled 1—same as red line after several weeks of storage in the freezer; G60 sample (dark blue line) and 1 LB film MOF coated Si63 wafer soaked overnight in 1.5 μmol/L PFOS (light blue line). Different regions of the spectra (**a**–**e**) and the entire specter (**f**) are shown.

The equilibrium spreading pressure (ESP) of the MOF MIL-101(Cr) was measured by placing some powder at the air–water interface while recording the surface pressure. The ESP was equal to 0 mN/m at 22 °C, indicating that the Langmuir film is in a metastable state above this pressure. Thus, e.g., the isotherm and the collapse pressure strongly depend on the barrier compression speed. Further on, on spreading of the Langmuir film, some substance goes under the layer, although an untypically high waiting time (40 min and more) was allowed for the solvent to evaporate. This can be seen by compressing the same layer a day later and observing an increase in layer area. The Langmuir film isotherms at room temperature with and without AA are shown in Figure 3. The surface pressure of the isotherm of the MIL-101(Cr) + 3% AA starts to increase at around 160 cm^2/mg. No phase transitions in the liquid-expanded phase can be distinguished. The isotherms are similar to the one reported earlier [26]. The collapse pressure for the pure MOF film is around 25 mN/m on very slow compression and around 30 mN/m when AA is added. Both these values are significantly lower than the observed collapse above 40 mN/m [26]. Also, the areas at which the surface pressure starts to increase are smaller in our case. Both differences can be attributed to our much larger MOF crystals, around 300–400 nm, compared to an average of 51 nm MIL-101(Cr) crystals in [26]. Larger crystals contribute to lower film stability and collapse at lower pressures. Also, the mass per unit area at the air-water interface is larger. The phase transition of AA at 25.6 mN/m from the liquid-expanded to the solid-expanded phase could not be observed and is masked by the MOF. The layer was not homogeneous on the air-water interface, and the deposited LB layers were a bit patchy. Further optimization of the type of matrix molecules used and their concentration, film heat treatment, use of counterions, etc., is needed and subject to future work.

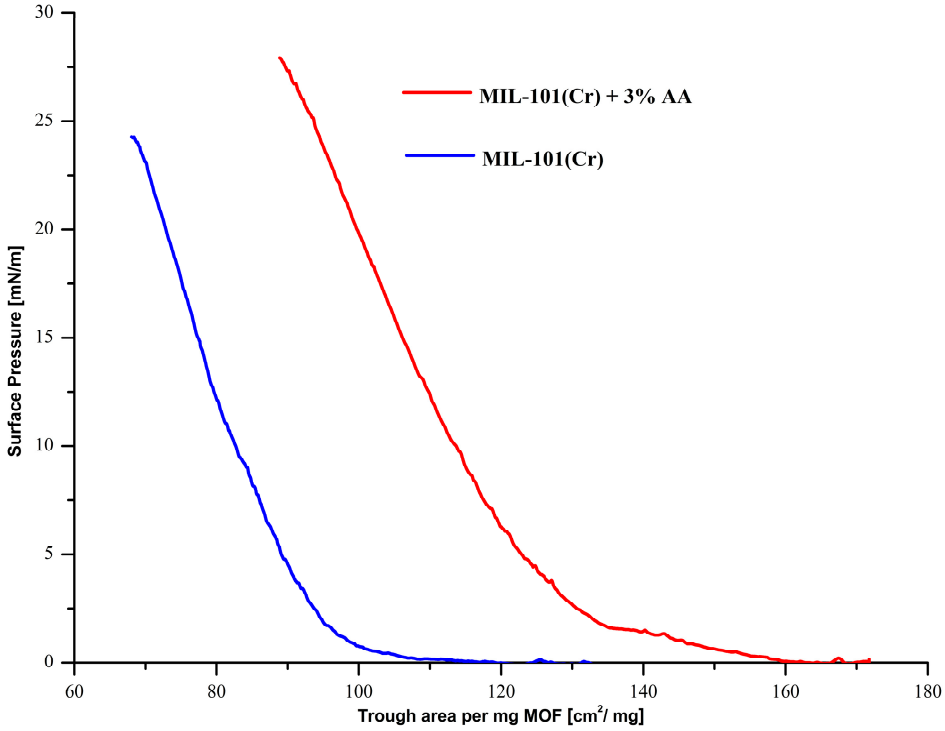

Figure 3. Langmuir film isotherms from a pure MIL-101(Cr) film (blue) and with 3% by volume added AA (red).

Different LB film deposition surface pressures and up to nine LB film layers were tested. Details about the film behavior at the air–water interface and on the solid support, the deposition process, and optimization are not within the scope of this paper. Thicker layers should provide higher sensor sensitivity due to the more absorption centers in the thicker MOF film. However, this decreases both the resonator's Q-factor and the reaction time due to the longer diffusion length for the analyte. Here, we present results for a SAW resonator coated with one LB layer at a lower pressure of 10 mN/m (samples G60 and G62). The film is more flexible at this lower surface pressure and should better bend around the 100 nm high interdigitated microelectrodes. In the case of EIS in a two-electrode configuration, we wanted maximum sensitivity from more deposited material. So, five LB layers at a higher surface pressure of 20 mN/m were deposited as the Q-factor was unimportant for this transduction method (see below). The 434 MHz SAW resonator was, on average, six times more sensitive to mass change than the 100 MHz QCM resonator, comparing air measurements on simultaneously deposited LB films. So, more layers were deposited on the QCM. The Q-factor of the SAW resonator was around 2800 on an uncoated resonator and dropped down to 1400 on one LB layer coating and 1.2 µmol/L PFOS adsorption. This is just a little above the threshold we have set for sensor applications [47]. The uncoated QCM measured at 300 MHz has a Q-factor of around 16,900 in air. On the first LB layer deposition, this value even goes slightly up, but on immersion in a buffer, the Q-factor drops to 200. So, the QCM can better tolerate LB films, and consequently, we deposited more LB film layers at higher surface pressure for a denser film to increase the sensitivity needed in the liquid environment testing. It should be noted that the LB films were very stable on interaction with liquids. In some cases, the layers were deposited simultaneously on flat gold substrates for electrical measurements and on ultra-flat Si wafers for AFM measurements. In the following notation in the paper, the letter G stands for SAW resonator samples (from surface-generated acoustic waves), not to be confused with the letter S, which stands for the Si wafer samples.

Figure 4 shows the topography measured using the AFM of one LB layer Si55 deposited simultaneously with the first layer of G55 at 20 mN/m. The layers are not smooth,

which can be expected with MOF crystals in the 300–400 nm range. The XPS data confirm that no MIL-101(Cr) passes through a 0.2 µm filter, so this large roughness can be expected. However, no macro holes are observed in the layer, which, if present, will shorten the signal in electrical measurements.

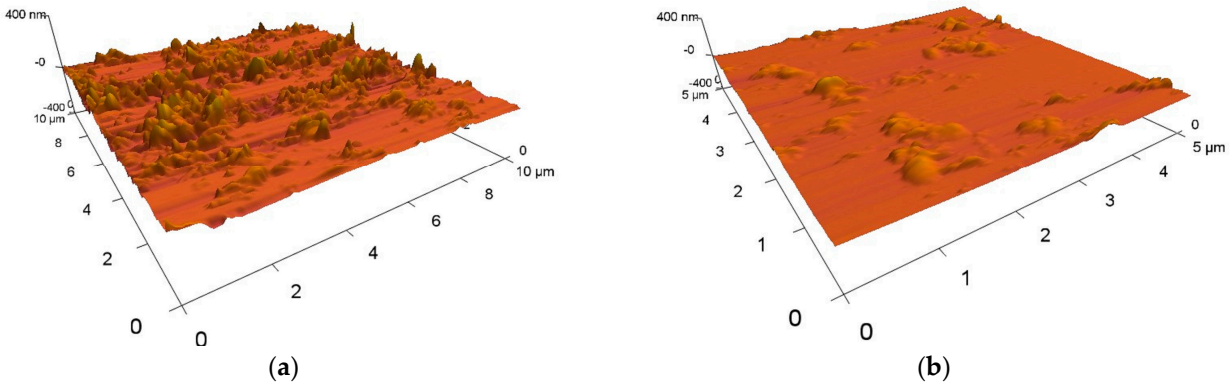

Figure 4. Three-dimensional topography of the surface of 1 LB layer from MIL-101(Cr) deposited on an ultra-flat Si wafer at 20 mN/m surface pressure simultaneously with G55 sample: (**a**) 10 µm scan; (**b**) 5 µm scan.

Initially, we tried gravimetric PFOS detection with the 100 MHz QCM covered with five LB MIL-101(Cr) layers. The PocketVNA can measure up to 4 GHz. So we measured the first harmonic at 100 MHz, the third harmonic at 300 MHz, the fifth harmonic at 500 MHz, the seventh harmonic at 700 MHz, and the ninth harmonic at 900 MHz. The dissipation can be calculated from these data. The third harmonic, as expected, has the strongest signal with the highest Q-factor, so we measure at this harmonic. We believe we are the first group to measure high-fundamental frequency (HFF) QCMs at such a high frequency. In the approximation of a rigid thin film, the frequency downshift Δf related to the sensor sensitivity is proportional to the square of the fundamental frequency (the Sauerbrey equation). Thus, a 100 MHz QCM should be 400 times more sensitive than the 5 MHz QCM. Part of the results for sample QCM53 deposited at a surface pressure of 28 mN/m, just below the film collapse with MOF one LB layer measured at its first harmonic on PFOS loading, are shown in Figure 5.

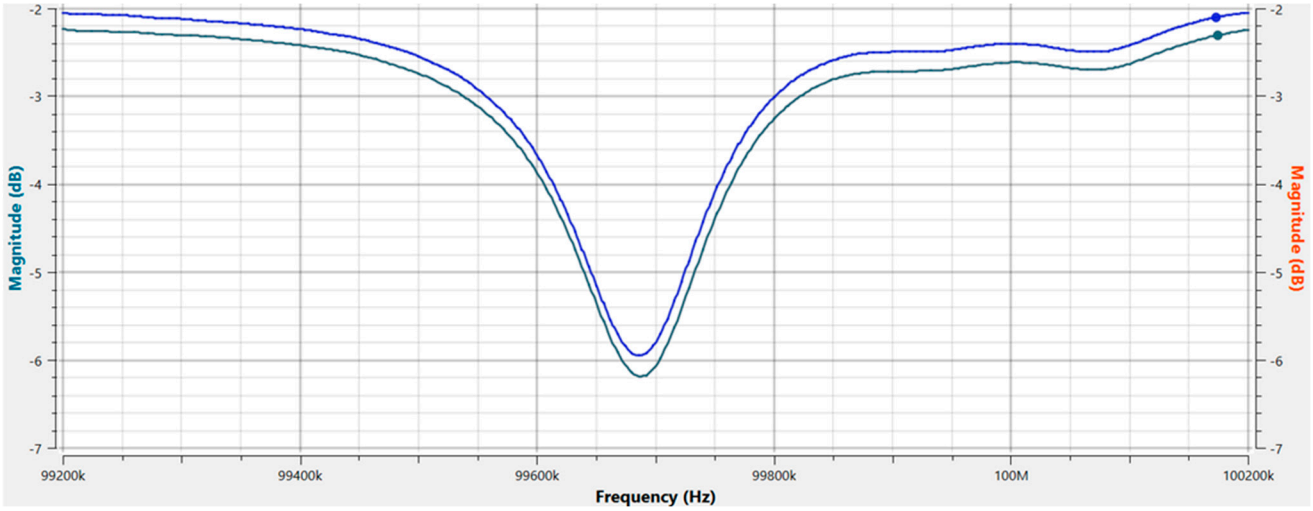

Figure 5. Gravimetry of sample QCM53 with 1 LB layer from MIL-101(Cr) deposited at a surface pressure of 28 mN/m in PB buffer. The lower green curve is without PFOS, while the upper blue curve is with 5 µmol/L PFOS. It is a little to the left, showing more adsorbed mass, but there was no monotonic change in the frequency downshift on the PFOS concentration increase.

Figure 6a shows gravimetric results for the QCM55 with five MOF LB layers tested in PB buffer at some of the different PFOS concentrations we used. The table in Figure 4b shows peak detection results using Origin 8.5 software from smoothed data.

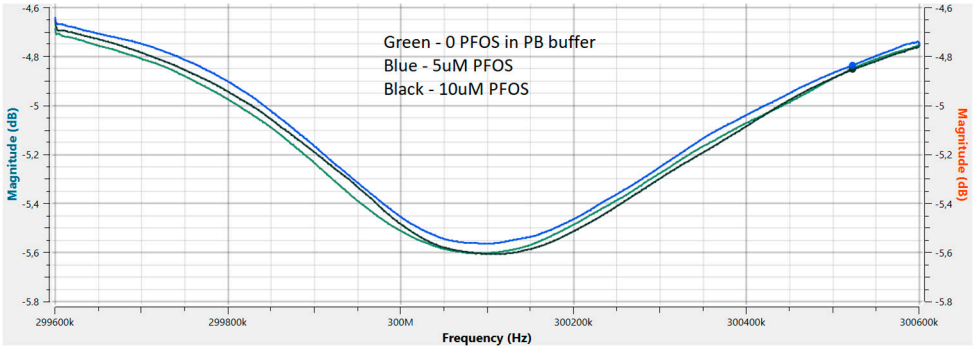

(**a**)

Sample QCM55	
PFOS conc. [µmol/L]	Peak mini-mum [MHz]
0	300.107
0.5	300.085
2	300.082
5	300.099
10	300.095

(**b**)

Figure 6. Gravimetry of sample QCM55 with 5 LB layers from MIL-101(Cr) deposited at a surface pressure of 20 mN/m in PB buffer: (**a**) graphic presentation of some of the results; (**b**) table of the resonance peak minimums for different PFOS concentrations No monotonic resonance frequency downshift is observed on the PFOS concentration increase.

These results indicate that no monotone QCM resonance frequency peak downshift was observed within the experimental error on increasing PFOS concentrations, as expected if more and more PFOS mass is adsorbed into the MIL-101(Cr) pores. Initially, at 0.5 and 2 µmol/L PFOS concentrations, there is a slight resonance frequency downshift from the pure water test, indicating some adsorbed mass. But already at 5 µmol/L PFOS concentrations, the resonance frequency upshifts, oppositely to what should be expected. Previous research suggests that this MIL-101(Cr) selectively adsorbs PFOS. Even tests with PFOS-spiked groundwater indicated selective PFOS capture by this MOF [39]. We also tested the MIL-101(Cr) selectivity against SDS and PFOA (see below). So, we can assume that the MOF layer selectively captures PFOS. However, the minimal adsorbed PFOS mass is masked by the much larger buffer or water mass captured in the MOF pores. Thus, the results were inconclusive for any gravimetric loading of these very sensitive QCM resonators in a liquid environment (PB buffer in this case) with PFOS concentrations in the µmol/L range. No wonder there are no papers in which gravimetry has been used for PFAS testing in liquids. There is one recent study [48] in which a couple of PFAS chemicals' adsorption isotherms on superparamagnetic iron oxide nanocrystals were tested with a QCM. However, the concentrations were in the mmol/L range, and minimal selectivity was observed. The frequency downshifts were only in the 20 to 60 Hz range.

The lack of a systematic resonance frequency downshift on PFOS water loading tested with one of the most sensitive QCMs on the market led us to try another gravimetric device and change the test protocol. First, we used two-port 434 MHz SAW resonators with gold electrodes specifically designed for sensor applications. For Rayleigh-type SAW resonators, the liquid environment cancels the signal. So secondly, we developed a protocol in which the SAW resonator was immersed in pure water spiked with different PFOS concentrations for a fixed amount of time (46 min), followed by expedited drying in warm air for 75 min.

Results for the G60 sample (1LB MIL-101(Cr) layer deposited at 10 mN/m) are shown in Figures 7 and 8 with identical scales and color coding and in Table 1. The first LB film layer mass with probably some contamination in it was 1.4 ng, which, after rinsing with water for 46 min, remains 0.89 ng. Both some contamination and the MOF layer that was not firmly attached had been removed. This mass is only approximately 25% of the mass of an AA LB monolayer deposited on the same resonator but at more than double the surface pressure of 22 mN/m and hence a higher density [47]. This observation, combined with

the much rougher surface of the MOF layer with hundreds of nanometer-sized features, confirms the very low density of MIL-101(Cr) due to its highly porous structure. The lower adsorbed mass at 0.2 µmol/L (Figure 7), compared to the subsequent 0.2 µmol/L PFOS steps, is probably due to the further layer cleaning during the 46 min rinsing with stirring at this concentration. After all the adsorptions, the loaded Q_L factor remains above 1000, which we had set as a lower limit for optimum sensor performance [47].

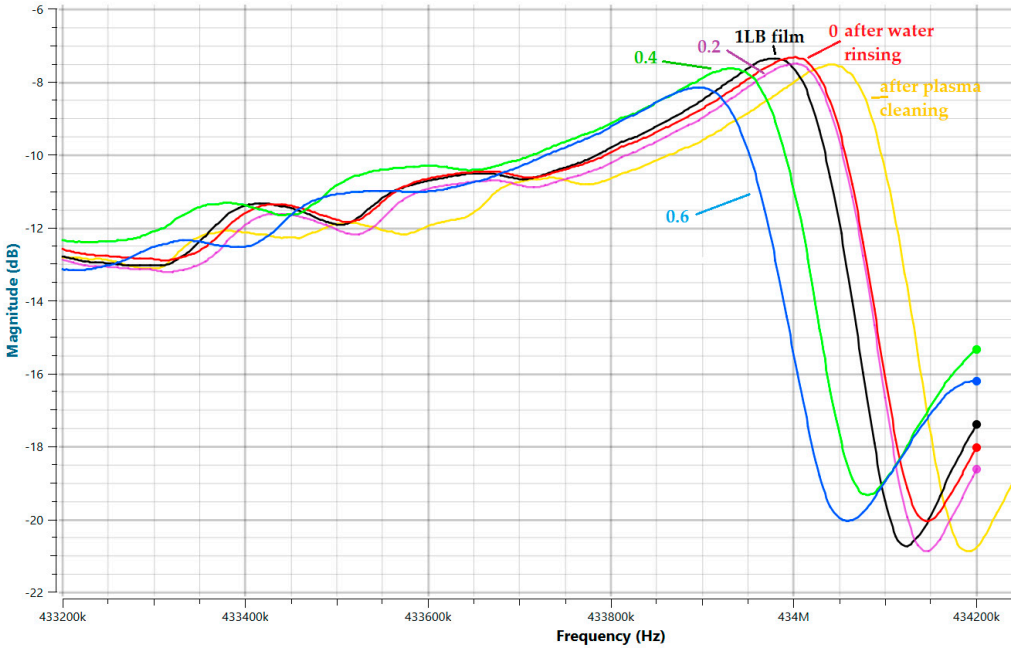

Figure 7. Gravimetric resonance peaks for sample G60 SAW 1 LB film MIL-101(Cr) covered 434 MHz resonator: yellow—150 min after plasma cleaning; black—after 1 LB film; red—after pure water rinsing; purple—with 0.2 µmol/L PFOS; green—with 0.4 µmol/L PFOS; blue—with 0.6 µmol/L PFOS.

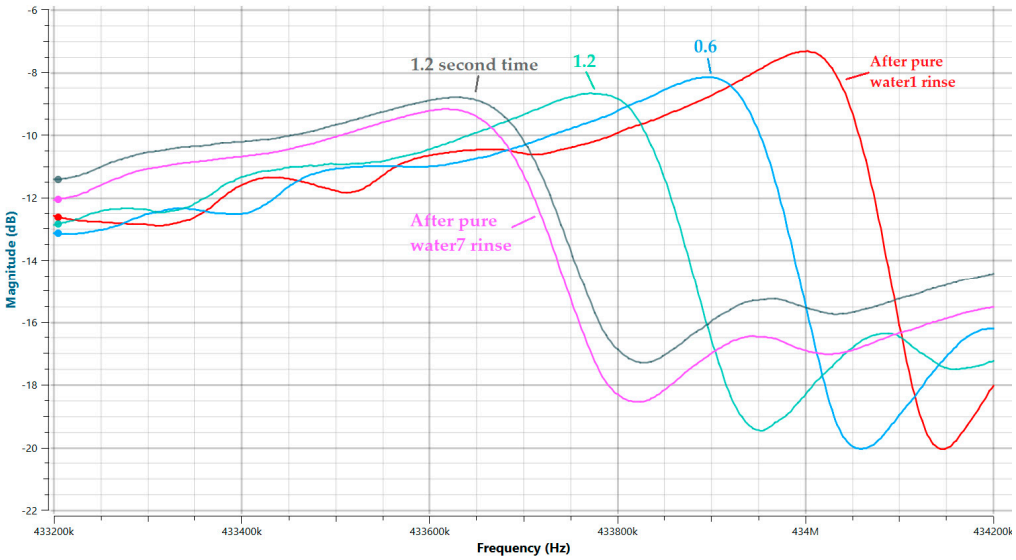

Figure 8. Gravimetric resonance peaks for sample G60 SAW 1 LB film MIL-101(Cr) covered 434 MHz resonator: red—after pure water rinsing; blue—with 0.6 µmol/L PFOS; green—with 1.2 µmol/L PFOS; gray—after a second 1.2 µmol/L PFOS immersion; purple—after pure water rinse to test contaminant accumulation.

Table 1. Summary of gravimetric data for the G60 sample 434 MHz SAW resonator coated with 1 LB film layer from MIL-101(Cr) at a surface pressure of 10 mN/m.

	Resonance Frequency f_0 [MHz]	Frequency Shift Δf [kHz]	Loaded Mass [ng] m = Δf/43.5	Group Delay τ_g [µs]	Loaded Q_L-Factor $Q_L = \pi f_o \tau_g$
After plasma	434.042	0	0	2.10	2862
1 LB film	433.981	−61	1.40	2.06	2807
Water1—pure	434.003	+22	0.51	2.10	2862
Water2 + 0.2 µmol/L PFOS	434.001	−2	0.046	2.04	2781
Water3 + 0.4 µmol/L PFOS	433.936	−65	1.49	1.80	2453
Water4 + 0.6 µmol/L PFOS	433.898	−38	0.87	1.75	2384
Water5 + 1.2 µmol/L PFOS	433.780	−118	2.71	1.54	2097
Water6 + 1.2 µmol/L PFOS again	433.636	−144	3.24	1.09	1484
Water7—pure	433.626	−10	0.23	1.05	1430
Water8 + 1.2 µmol/L dodecyl sulfate	433.620	−6	0.14	0.64	872

The insertion loss decreases minimally from 7.4 to 8.3 dB. The frequency downshift between 0.2 and 1.2 µmol/L concentrations is 221 kHz (Table 1). Compared to the downshifts typically measured with QCMs in the 10 to 60 Hz range, e.g., [48], it indicates the achievable signal purity and peak detection accuracy with modern, specialized, 100 times more expensive instrumentation and dedicated resonance peak detection software. Our experiments use a general-purpose pocket-sized VNA at a EUR 500 price range with a much higher than required by us scan range (4 GHz, and consequently smaller accuracy) and no specialized peak detection software. However, there is work in progress on peak detection. Thermostation of the sample can also significantly improve signal accuracy and stability. So, instrumentation-wise, there is a significant margin for improvement. Sensor sensitivity can be further enhanced considerably if the resonator is included in a sensor oscillator circuit, resulting in several orders of magnitude improvements in the LOD [45,46]. Thus, the proposed gravimetric method of PFOS detection could be capable of determining concentrations required by the water purity legislation for PFAS contaminants. The SAW resonators used measure approximately 2 × 3 mm, and the electrodes are on one side and thus are much more suitable for system integration and miniaturization for in-field applications than alternative transduction techniques like electrochemical or optical methods and QCMs. SAW resonators are also much more robust devices.

Three control experiments were performed to check the validity of the results. First, an uncoated sample G61 was plasma-cleaned and then tested by immersing it in pure water, followed by drying with and immersion in 1.2 µmol/L PFOS concentration solution for 46 min each (Figure 9). After drying from pure water, there was a 54 kHz frequency downshift. This can be due to some water contamination as the water quality was far from excellent. Alternatively, this can also be due to the effects of plasma cleaning. On this sample, the plasma cleaning resulted in a 205 kHz frequency upshift (not shown), which was moving up for almost 5 h before stabilization. The effects of the air plasma on this microelectrode structure are poorly understood, but immersing in water could have removed part of this effect. More importantly, on a subsequent immersion in 1.2 µmol/L PFOS solution, the lack of frequency downshift indicated no PFOS influence on a bare resonator.

In a second control experiment, we immersed the G60 sample in 1.2 µmol/L of SDS solution (Figure 10). This compound is similar to the tested PFOS, but the fluorine atoms are replaced with hydrogen atoms, and the chain is a bit longer. There was only some 6 kHz frequency downshift, which can be due to water contamination, e.g., the pure water rinse caused a 10 kHz downshift. This minimal downshift should be compared to the 144 kHz downshift on the second immersion in 1.2 µmol/L PFOS solution.

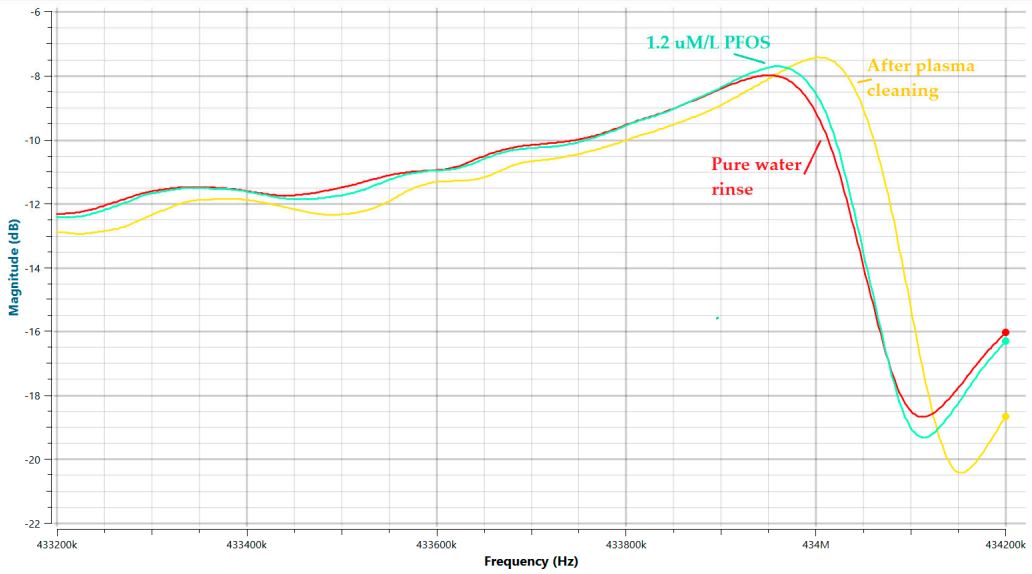

Figure 9. Gravimetric resonance peaks for sample G61 SAW 434 MHz resonator without any coating: yellow—after plasma cleaning and relaxation for 280 min; red—after pure water rinsing; green—with 1.2 µmol/L PFOS. Results show that PFOS does not affect an uncoated resonator.

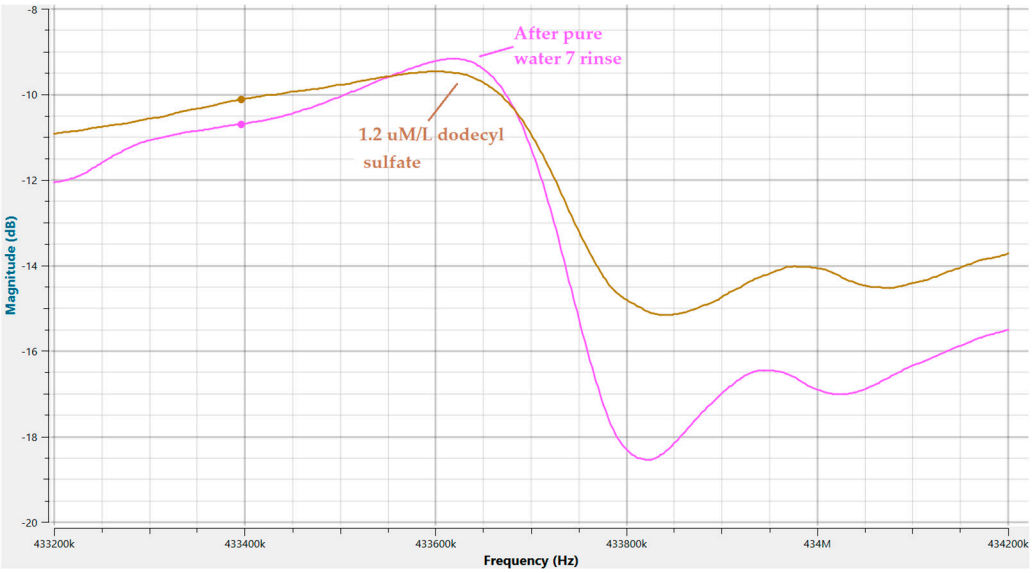

Figure 10. Gravimetric resonance peaks for sample G60 SAW 1 LB film MIL-101(Cr) covered 434 MHz resonator: purple—after pure water rinse; brown—in 1.2 µmol/L sodium dodecyl sulfate (SDS), a very similar to PFOS compound. The minimum downshift indicates no adsorption and, consequently, the high selectivity of this MOF coating to PFOS.

In a third control experiment, a newly prepared G62 sample on the single LB film from MIL-101(Cr) was deposited at the same surface pressure of 10 mN/m as the G60 sample and was tested against 1.2 µmol/L of PFOA. This PFAS contaminant is similar to PFOS but with a different head group. More MIL-101(Cr) mass was deposited compared to G60, although at the same surface pressure due to the above-mentioned film inhomogeneity. But this should produce a higher sensitivity device. However, there was no frequency downshift due to PFOA adsorption at all (Figure 11). These results confirm the high selectivity of the MIL-101(Cr) coating to PFOS.

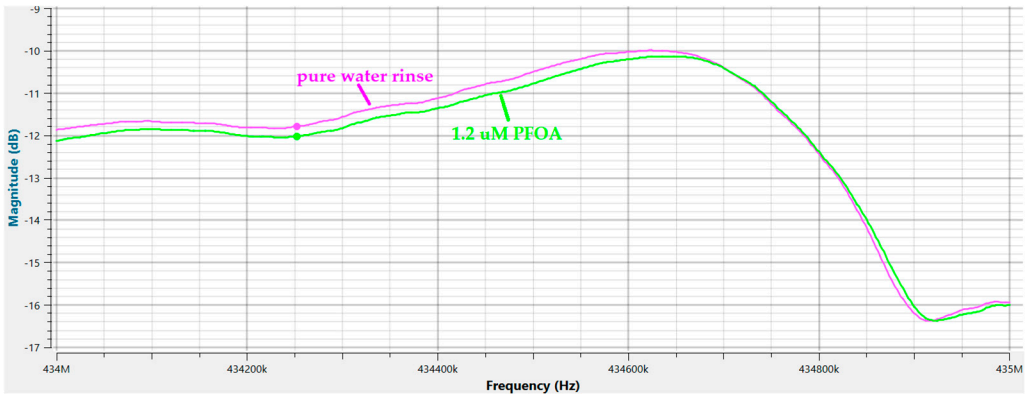

Figure 11. Gravimetric resonance peaks for sample G62 SAW 1 LB film at 10 mN/m MIL-101(Cr) covered 434 MHz resonator: purple—after pure water rinse; green—in 1.2 µmol/L PFOA, a very similar to PFOS compound. The lack of downshift indicates no adsorption and, consequently, the high selectivity of this MOF coating to PFOS.

As an additional transduction method for PFOS detection, EIS has been tested in a PB buffer. We used a three-electrode configuration with an Ag/AgCl reference electrode and a platinum coil counter electrode. As working electrodes were used MIL-101(Cr) coated by the LB layers flat gold samples with an approximate area of the SMD-mounted SAW resonators. The MOF-covered SAW resonators were tested in either a three-electrode configuration in which the two interdigitated electrodes are shorted and used as a working electrode or a two-electrode cell configuration in which there is no reference electrode, but the reference input of the potentiostat is connected to the counter electrode. The working and counter electrodes are connected to one of the pairs of interdigitated and ground electrodes of the two-port resonator. Preliminary data for this last configuration is reported here (Figure 12).

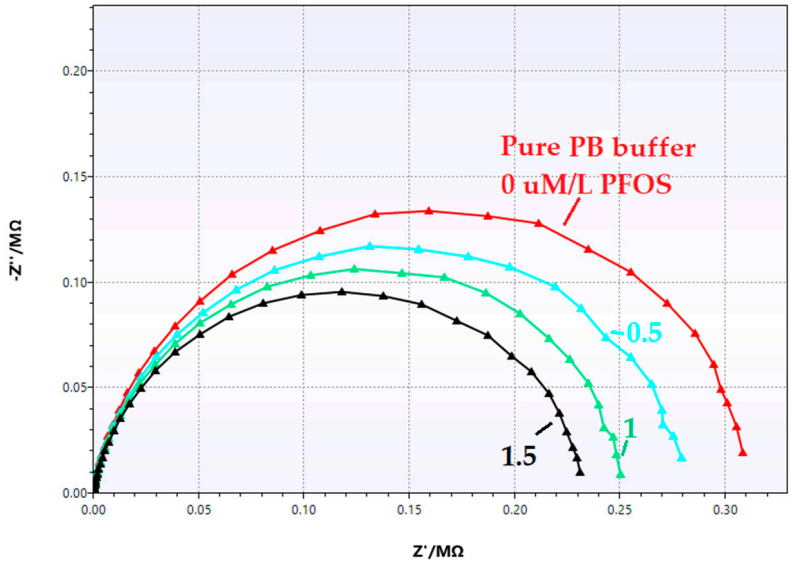

Figure 12. A Nyquist plot from the EIS data measured in a two-electrode configuration between the interdigitated electrodes of sample G55 with five LB layers from MIL-101(Cr) deposited at a surface pressure of 20 mN/m covered SAW resonator in a PB buffer at different PFOS concentrations: red—no PFOS; blue—0.5 µmol/L PFOS; green—1 µmol/L PFOS; black—1.5 µmol/L PFOS.

The elimination of the reference electrode cancels the 10 kHz maximum frequency limit imposed by its slow reaction time, so we tested the EIS to 1 MHz frequency. An additional advantage of the lack of a reference electrode is the much easier integration for

in-field applications. Using a large number of microelectrode-sized electrodes (5 µm width) gives a much higher signal-to-noise ratio [49]. Additionally, the interdigitated microelectrodes (IDµEs) as electrochemical transducers offer the added advantage of high collection efficiencies, a low response time that favors rapid detection, low ohmic drop, and readiness for miniaturization [39]. The sensing layer symmetrically covers both electrodes, and specific reactions occur on both of them [50].

EIS measurements usually provide information on electron transfer processes, which, in our case, demonstrate the adsorption of PFOS onto five LB layers covered with the MOF MIL-101(Cr) SAW resonator. Impedance is a measure of the ability of a circuit to resist the flow of electrical current, and the real part (Z') of the impedance spectra in the Nyquist plot highlights its resistive behavior. In the air, the structure behaves as a pure capacitor, situated between the 100 nm-high, 5 µm-spaced IDµEs covered by the excellent dielectric that MIL-101(Cr) is. Resistances reach above 10 GΩ below 10 Hz frequencies. The semicircle shape of the Nyquist plots in the buffer corresponds to a direct electron transfer limited process [51]. The greater the radius of the semicircle, the greater the resistance, suggesting a decrease in the electron transfer. Since PFOS carries a −1 charge at the pHs used, the reduction in resistance highlights the adsorption of PFOS, whose presence in the MOF pores increases the electron transfer through the LB layer. Detailed discussion of the electrochemical data is outside this paper's scope.

We proved that we could combine gravimetric data and EIS data on a single device, a SAW resonator. While this is typical in E-QCM applications, the gravimetric data here are unprecedentedly sensitive to small molecules adsorbed from a liquid environment. On the other hand, the SAW resonator IDµEs provide significant signal improvement for the EIS measurements. EIS in this configuration could be easily measured in highly purified water with sensor resistances within the 5 MΩ range at 0.05 Hz, which is accessible for handheld and pocket tablet-operated potentiostats. Thus, the entire system can be used for in-field real-time PFOS contamination monitoring. To reach the 0.1 µg/L PFAS detection legislative limits, improvements are needed in instrumentation (specialized VNA with integrated peak detection software, sensor oscillator circuitry), MOF LB film understanding and optimization, sensing layer selectivity and manipulation through, e.g., MOF modification [52], and test protocol modifications. However, the frequency downshifts reported here of around 220 kHz per 1 µmol/L = 0.5 mg/L of PFOS, with a resonator-loaded Q_L factor above 2000 and reaction times in the minutes range, are highly promising. The limit of detection (LOD) for this method at its current implementation is limited by the instrument detection limit (IDL). The standard peak deviation for our pocket-sized VNA device when measuring the 434 MHz SAW resonance peaks without averaging and any optimization was measured to be 1 kHz. This would give an LOD of around 7 µg/L. The manufacturer of the VNA we used claims that 100 Hz precision was obtained for a 400 MHz resonator [53], which would give an LOD of 0.7 µg/L. At the same time, a commercial QCM-D device for 5 MHz resonators specifies a frequency noise of only 0.03 Hz [54]. This instrument uses an exponential decay-based characterization electronic oscillator system introduced in 1996 [55]. A later development in electronics suggests phase-shift monitoring resulting in a three times signal-to-noise ratio improvement at 10 MHz, expected to perform even better at higher frequencies [56]. SAW oscillator electronics design has also been investigated [57]. Although the noise is proportional to the frequency of the resonator, with targeted instrument development it should be possible to cover the legislative sensitivity requirements for PFAS detection.

The best in situ device for PFOS detection currently has an LOD of 0.5 ng/L [39]. It uses the same MIL-101(Cr) after a special activation protocol. The MOF is placed in a cylindrical microfluidic channel sandwiched between 3D-spaced microelectrodes. EIS is used as a transduction mechanism. However, the device requires pumping water for 3 h before reaching a baseline. This is a form of solid-phase extraction. The design makes its in-field application problematic. This device is reusable by simply passing pure water through the microfluidic channel again for 3 h. In our case, we could only partially remove

the adsorbed mass by washing it in pure water. Even washing at 43 °C, a temperature below the AA tail melting point, could not restore the resonant frequency value before PFOS loading. We are exploring this problem, especially since MIL-101(Cr) is among the best-studied MOFs [58]. The possibilities for electrochemical oxidation and electrocatalytic degradation of the PFAS should also be considered [59]. The closely spaced, only 5 μm from each other, interdigitated electrodes are very suitable for providing high electric fields even at small external voltages.

One approach to increase the sensitivity toward PFAS is fluorine functionalization [52,60]. A few other papers using different MOF molecules for PFAS detection are worth mentioning [61–63]. Optical or microextraction mass spectrometry was used to transduce the signal. In a just-published paper, silver nanoparticles embedded within a fluorine-rich Ti_3C_2-based multilayered MXene were binding several PFAS contaminants and showed specificity of the sensor for long-chain PFAS, and no interferences from structurally similar compounds lacking F, small molecules, organic matter, and ions. EIS was used, and a very low LOD of 33 ppq was achieved [64]. However, the measurements were performed in PBS buffer with $Fe(CN)_6^{3-/4-}$ redox probe, which questions constant water monitoring applications. An excellent result in PFOS sensing with an LOD of 7.5 ng/L was achieved by using the MIP approach [65]. A thin coating of gold nanoparticles with a well-developed dendritic structure was drop-cast on a glassy carbon electrode. This helps increase the voltammetric response to a Fe redox probe. On top, this structure was covered with electropolymerized MIP. A novel statistical approach was used to simultaneously optimize the three significant factors influencing the sensitivity—CV cycles, the monomer/template ratio, and electrolyte pH. PFOS concentrations in the 0.05 nmol/L to 1 μmol/L range were tested with very high selectivity. The sensor reusability was not discussed. While showing impressive sensitivity, this sensor would be challenging to use for constant in-field water purity monitoring. The gravimetric sensing concept we suggest does not need any additional chemical additives or pH regulation. The SAW resonator can be automatically immersed in the water to be tested for a definitive amount of time and then withdrawn and the Peltier element heated for faster drying and maintenance at constant temperature for precision data reading. The sensor should be covered with an anti-fouling coating for long-term use. Thus, the gravimetric detection concept of small-sized molecules dissolved in water presented here is very promising for in-field continuous water purity monitoring.

4. Conclusions

In this work, we have shown that even the usage of a very sensitive 100 MHz QCM measured at the third harmonic could not detect a small-sized molecule like PFOS (MW 500) in μmol/L concentrations gravimetrically in a liquid environment because the mass of the adsorbed liquid masks its mass. Instead, we proposed to use a more sensitive two-port 434 MHz SAW resonator with gold electrodes. We immerse the resonator in pure water spiked with PFOS at different concentrations, wait for 46 min, then dry the resonator and measure the resonance frequency downshift and Q-factor change. Thus, we have demonstrated the first gravimetric detection of PFOS, or more generally—of such small molecules in water. Gravimetric detection is considered the gold standard in chemical sensing as there is no need for data interpretation. We used the MOF MIL-101(Cr), which is known to be selective toward PFOS adsorption, for the resonator's sensing layer. Its selectivity was tested with SDS and PFOA. The discreet layer-by-layer LB method carried out the sensing layer deposition. The achieved estimated LOD is still a couple of orders of magnitude higher than the PFAS EU legislative requirements for water intended for human consumption. This could be improved by using dedicated measuring electronics, optimizing the sensing layer coating, using smaller-sized MOF crystals, and eventually, functionalizing them. Additionally, we have proven that the electrodes of the SAW resonator can be used for a two-electrode EIS spectroscopy detection of PFOS. Combining two complementary transduction mechanisms on a single device gives additional sensor selectivity. These results are an important step forward in developing in-field sensors for

constantly monitoring water quality. While here we focus on one of the emerging water contaminants, this concept with a different selective coating can be used for other new contaminants like microcystin-LR or secondary water contamination, e.g., from dissolved medical drugs in the wastewater to be reused.

Supplementary Materials: The following supporting information can be downloaded at https://www.mdpi.com/article/10.3390/chemosensors12070116/s1: Figure S1: Nitrogen adsorption-desorption for MIL-101(Cr) used in this study. Figure S2: X-ray diffraction (XRD) for the powder raw MIL-101(Cr) material.

Author Contributions: Conceptualization, G.R.I.; methodology, G.R.I., M.F., M.D., Y.G.M., G.B.H. and A.T.; investigation, G.R.I., S.K, T.V. and G.B.H.; resources, G.R.I., M.F., Y.G.M. and A.T.; data curation, G.R.I., T.V., S.K., M.D., M.F., Y.M., G.B.H. and A.T.; writing—original draft preparation, G.R.I. and T.V.; writing—review and editing, G.R.I., T.V., M.F., M.D., G.B.H. and S.K.; visualization, G.R.I., S.K. and M.D.; supervision, G.R.I.; project administration, G.R.I. and Y.G.M.; funding acquisition, G.R.I. All authors have read and agreed to the published version of the manuscript.

Funding: This research was funded by the Bulgarian National Science Foundation, grant number KP-06-N 68/3, and the Center for Research and Design, University of Architecture, Civil Engineering and Geodesy, grant number BN-289/23.

Institutional Review Board Statement: Not applicable.

Informed Consent Statement: Not applicable.

Data Availability Statement: The raw data supporting the conclusions of this article will be made available by the authors on request.

Acknowledgments: The AFM used in this study was part of the Distributed Research Infrastructure INFRAMAT, part of the Bulgarian National Roadmap for Research Infrastructures, supported by the Bulgarian Ministry of Education and Science.

Conflicts of Interest: The authors declare no conflicts of interest. The funders had no role in the design of this study; the collection, analyses, or interpretation of data; the writing of the manuscript; or the decision to publish the results.

References

1. Amin, M.; Sobhani, Z.; Liu, Y.; Dharmaraja, R.; Chadalavada, S.; Naidu, R.; Chalker, J.; Fang, C. Recent advances in the analysis of per- and polyfluoroalkyl substances (PFAS)—A review. *Environ. Technol. Innov.* **2020**, *19*, 100879. [CrossRef]
2. Boiteux, V.; Dauchy, X.; Rosin, C.; Munoz, J.-F. National screening study on 10 perfluorinated compounds in raw and treated tap water in France. *Arch. Environ. Contam. Toxicol.* **2012**, *63*, 1–12. [CrossRef] [PubMed]
3. Directive (EU) 2020/2184 of the European Parliament and of the Council of 16 December 2020 on the Quality of Water Intended for Human Consumption. Available online: https://eur-lex.europa.eu/eli/dir/2020/2184/oj (accessed on 15 April 2024).
4. USA EPA. Drinking Water Health Advisories for PFOA and PFOS, 15 June 2022. Available online: https://www.epa.gov/sdwa/drinking-water-health-advisories-pfoa-and-pfos (accessed on 7 April 2024).
5. Bell, E.; De Guise, S.; R McCutcheon, J.; Lei, Y.; Levin, M.; Li, B.; Rusling, J.; Lawrence, D.; Cavallari, J.; O'Connell, C.; et al. Exposure, health effects, sensing, and remediation of the emerging PFAS contaminants—Scientific challenges and potential research directions. *Sci. Total Environ.* **2021**, *780*, 146399. [CrossRef]
6. Garg, S.; Kumar, P.; Greene, G.; Mishra, V.; Avisar, D.; Sharma, R.; Dumee, L. Nano-enabled sensing of per-/poly-fluoroalkyl substances (PFAS) from aqueous systems—A review. *J. Environ. Manag.* **2022**, *308*, 114655. [CrossRef] [PubMed]
7. Tabar, F.; Lowdon, J.; Sichani, S.; Khorshid, M.; Cleij, T.; Diliën, H.; Eersels, K.; Wagner, P.; van Grinsven, B. An Overview on Recent Advances in Biomimetic Sensors for the Detection of Perfluoroalkyl Substances. *Sensors* **2024**, *24*, 130. [CrossRef]
8. Petty, M. *Molecular Electronics: From Principles to Practice*; John Wiley & Sons Ltd.: Chichester, UK, 2007; ISBN 978-0-470-01307-6.
9. Gaikar, P.; Sangale, S.; Wadhawa, G. The Langmuir-Blodgett method for metal oxide nanostructures. In *Metal Oxides, Solution Methods for Metal Oxide Nanostructures*; Mane, R., Jadhav, V., Al-Enizi, A., Eds.; Elsevier: Amsterdam, The Netherlands, 2023; pp. 369–392. ISBN 9780128243534. [CrossRef]
10. Clark, R.; Dick, J. Towards deployable electrochemical sensors for per- and polyfluoroalkyl substances (PFAS). *Chem. Commun.* **2021**, *57*, 8121–8130. [CrossRef] [PubMed]
11. Glasscott, M.; Vannoy, K.; Kazemi, R.; Verber, M.D.; Dick, J. μ-MIP: Molecularly imprinted polymer-modified microelectrodes for the ultrasensitive quantification of GenX (HFPO-DA) in river water. *Environ. Sci. Technol. Lett.* **2020**, *7*, 489–495. [CrossRef]
12. Park, J.; Yang, K.; Choi, Y.; Choe, J. Novel ssDNA aptamer-based fluorescence sensor for perfluorooctanoic acid detection in water. *Environ. Int.* **2023**, *158*, 107000. [CrossRef]

13. Howarth, A.; Liu, Y.; Li, P.; Li, Z.; Wang, T.; Hupp, J.; Farha, O. Chemical, thermal and mechanical stabilities of metal-organic frameworks. *Nat. Rev. Mater.* **2016**, *1*, 15018. [CrossRef]
14. Ruiz, M.; Sua, A.; Tian, F. Covalent Attachment of Metal-Organic Framework Thin Films on Surfaces. In *Encyclopedia of Interfacial Chemistry*; Wandelt, K., Ed.; Elsevier: Amsterdam, The Netherlands, 2018; pp. 646–671. ISBN 9780128098943. [CrossRef]
15. Zhang, Y.; Chang, C.-H. Metal-Organic Framework Thin Films: Fabrication, Modification, and Patterning. *Processes* **2020**, *8*, 377. [CrossRef]
16. Crivello, C.; Sevim, S.; Graniel, O.; Franco, C.; Pané, S.; Puigmartí-Luis, J.; Muñoz-Rojas, D. Advanced technologies for the fabrication of MOF thin films. *Mater. Horiz.* **2021**, *8*, 168–178. [CrossRef] [PubMed]
17. López, Y.; Viltres, H.; Gupta, N.; Acevedo-Peña, P.; Leyva, C.; Ghaffari, Y.; Gupta, A.; Kim, S.; Bae, J.; Kim, K. Transition metal-based metal-organic frameworks for environmental applications: A review. *Environ. Chem. Lett.* **2021**, *19*, 1295–1334. [CrossRef]
18. Makiura, R. Creation of metal-organic framework nanosheets by the Langmuir-Blodgett technique. *Coord. Chem. Rev.* **2022**, *46915*, 214650. [CrossRef]
19. Tsotsalas, M.; Umemura, A.; Kim, F.; Sakata, Y.; Reboul, J.; Kitagawa, S.; Furukawa, S. Crystal Morphology-Directed Framework Orientation in Porous Coordination Polymer Films and Freestanding Membranes via Langmuir-Blodgettry. *J. Mater. Chem.* **2012**, *22*, 10159–10165. [CrossRef]
20. Makiura, R.; Motoyama, S.; Umemura, Y.; Yamanaka, H.; Sakata, O.; Kitagawa, H. Surface Nano-Architecture of a Metal-Organic Framework. *Nat. Mater.* **2010**, *9*, 565–571. [CrossRef] [PubMed]
21. Makiura, R.; Kitagawa, H. Porous Porphyrin Nanoarchitectures on Surfaces. *Eur. J. Inorg. Chem.* **2010**, *24*, 3715–3724. [CrossRef]
22. Benito, J.; Fenero, M.; Sorribas, S.; Zornoza, B.; Msayib, K.J.; McKeown, N.B.; Téllez, C.; Coronas, J.; Gascón, I. Fabrication of Ultrathin Films Containing the Metal Organic Framework Fe-MIL-88B-NH_2 by the Langmuir–Blodgett Technique. *Colloids Surf. A* **2015**, *470*, 161–170. [CrossRef]
23. Seoane, B.; Coronas, J.; Gascon, I.; Benavides, M.E.; Karvan, O.; Caro, J.; Kapteijn, F.; Gascon, J. Metal-Organic Framework Based Mixed Matrix Membranes: A Solution for Highly Efficient CO_2 Capture. *Chem. Soc. Rev.* **2015**, *44*, 2421–2454. [CrossRef] [PubMed]
24. Betard, A.; Fischer, R. Metal-Organic Framework Thin Films: From Fundamentals to Applications. *Chem. Rev.* **2012**, *112*, 1055–1083. [CrossRef]
25. Demessence, A.; Horcajada, P.; Serre, C.; Boissiere, C.; Grosso, D.; Sanchez, C.; Fereya, G. Elaboration and properties of hierarchically structured optical thin films of MIL-101(Cr). *Chem. Commun.* **2009**, 7149–7151. [CrossRef]
26. Benito, J.; Sorribas, S.; Lucas, I.; Coronas, J.; Gascon, I. Langmuir–Blodgett Films of the Metal-Organic Framework MIL-101(Cr): Preparation, Characterization, and CO_2 Adsorption Study Using a QCM-Based Setup. *ACS Appl. Mater. Interfaces* **2016**, *8*, 16486–16492. [CrossRef] [PubMed]
27. Haghighi, E.; Zeinali, S. Nanoporous MIL-101(Cr) as a sensing layer coated on a quartz crystal microbalance (QCM) nanosensor to detect volatile organic compounds (VOCs). *RSC Adv.* **2019**, *9*, 24460. [CrossRef] [PubMed]
28. Xie, D.; Wang, R.; Fu, J.; Zhao, Z.; Li, M. AuNPs@MIL-101 (Cr) as a SERS-Active Substrate for Sensitive Detection of VOCs. *Front. Bioeng. Biotechnol.* **2022**, *10*, 921693. [CrossRef] [PubMed]
29. Shen, Y.; Tissot, A.; Serre, C. Recent progress on MOF-based optical sensors for VOC sensing. *Chem. Sci.* **2022**, *13*, 13978. [CrossRef] [PubMed]
30. Mousavi, S.; Zeinali, S. VOC s detection using resistive gas nanosensor based on MIL-101(Cr) as a metal-organic framework. *Sens. Actuators A Phys.* **2022**, *346*, 113810. [CrossRef]
31. Li, Z.; Hu, J.; Xiao, Y.; Zha, Q.; Zeng, L.; Zhu, M. Surfactant assisted Cr-metal organic framework for the detection of bisphenol A in dust from E-waste recycling area. *Anal. Chim. Acta* **2021**, *1146*, 174–183. [CrossRef]
32. Haghighi, E.; Zeinali, S. Formaldehyde detection using quartz crystal microbalance (QCM) nanosensor coated by nanoporous MIL-101(Cr) film. *Microporous Mesoporous Mat.* **2020**, *300*, 110065. [CrossRef]
33. Wang, Q.; Shi, Z.; Wang, Z.; Zhao, Y.; Li, J.; Hu, H.; Bai, Y.; Xu, Z.; Hui, Z.; Wang, L. Rapid simultaneous adsorption and SERS detection of acid orange II using versatile gold nanoparticles decorated NH_2-MIL-101(Cr). *Anal. Chim. Acta* **2020**, *1129*, 126–135. [CrossRef]
34. Zhang, J.; Sun, L.; Chen, C.; Liu, M.; Dong, W.; Guo, W.; Ruan, S. High performance humidity sensor based on metal organic framework MIL-101(Cr) nanoparticles. *J. Alloys Compd.* **2017**, *695*, 520–525. [CrossRef]
35. Wu, M.; Ma, Z.; Fan, Y.; Wu, Y.; An, Z.; Zhao, H.; Liu, Y.; Xu, J. Materials Design, Sensing Performance and Mechanism of Anhydrous Hydrogen Fluoride Gas Sensor Based on Amino-Functionalized MIL-101(Cr) for New Energy Vehicles. *Coatings* **2022**, *12*, 260. [CrossRef]
36. Zhong, X.; Zhang, M.; Guo, L.; Xie, Y.; Luo, R.; Chen, W.; Cheng, F.; Wang, L. A dual-signal self-checking photoelectrochemical immunosensor based on the sole composite of MIL-101(Cr) and CdSe quantum dots for the detection of α-fetoprotein. *Biosens. Bioelectron.* **2021**, *189*, 113389. [CrossRef] [PubMed]
37. Liu, K.; Zhang, S.; Hu, X.; Zhang, K.; Roy, A.; Yu, G. Understanding the adsorption of PFOA on MIL-101 (Cr)-based anionic-exchange metal-organic frameworks: Comparing DFT calculations with aqueous sorption experiments. *Environ. Sci. Technol.* **2015**, *49*, 8657–8665. [CrossRef]

38. Chatterjee, S.; Motkuri, R.K.; Basuray, S.; Cheng, Y.H. Fluidic Impedance Platform for In-situ Detection and Quantification of PFAS in Groundwater. International Patent Application No. WO 2020/236435, 26 November 2020.
39. Cheng, Y.; Barpaga, D.; Soltis, J.; Shutthanandan, V.; Kargupta, R.; Han, K.; McGrail, B.; Motkuri, R.; Basuray, S.; Chatterjee, S. Metal−Organic Framework-Based Microfluidic Impedance Sensor Platform for Ultrasensitive Detection of Perfluorooctanesulfonate. *ACS Appl. Mater. Interfaces* **2020**, *12*, 10503–10514. [CrossRef]
40. Zhang, J.; Zhang, X.; Wei, X.; Xue, Y.; Wan, H.; Wang, P. Recent advances in acoustic wave biosensors for the detection of disease-related biomarkers: A review. *Anal. Chim. Acta* **2021**, *1164*, 338321. [CrossRef]
41. Mujahid, A.; Afzal, A.; Dickert, F. An Overview of High Frequency Acoustic Sensors—QCMs, SAWs and FBARs—Chemical and Biochemical Applications. *Sensors* **2019**, *19*, 4395. [CrossRef]
42. Balcerzak, A.; Kiełczyński, P.; Szalewski, M.; Wieja, K. SAW Sensor with Langmuir-Blodgett Layer for Detection of Benzene and its Derivatives. *Arch. Acoust.* **2021**, *46*, 25–30. [CrossRef]
43. Liang, R.; Wang, S.; Lu, Y.; Yan, G.; He, Z.; Xia, Y.; Liang, Z.; Wu, L. Assembling Ultrafine SnO_2 Nanoparticles on MIL-101(Cr) Octahedrons for Efficient Fuel Photocatalytic Denitrification. *Molecules* **2021**, *26*, 7566. [CrossRef] [PubMed]
44. Avramov, I.; Stahl, U. On the Mass Sensitivity of Rayleigh Surface Acoustic Wave (RSAW) Resonators. In Proceedings of the 40th International Spring Seminar on Electronics Technology (ISSE), Sofia, Bulgaria, 10–14 May 2017; pp. 1–6. [CrossRef]
45. Avramov, I.; Länge, K.; Rupp, S.; Rapp, B.; Rapp, M. Polymer coating behaviour of Rayleigh-SAW resonators with gold electrode structure for gas sensor applications. *IEEE Trans. Ultrason. Ferroelectr. Freq. Control* **2007**, *57*, 157–166. [CrossRef]
46. Avramov, I. The Quartz Surface Microbalance—A Possible Candidate for Rapid Respiratory Virus Detection. In Proceedings of the IEEE International Symposium on Applications of Ferroelectrics (ISAF), Sydney, Australia, 16–21 May 2021. [CrossRef]
47. Avramov, I.; Ivanov, G. Layer by Layer Optimization of Langmuir–Blodgett Films for Surface Acoustic Wave (SAW) Based Sensors for Volatile Organic Compounds (VOC) Detection. *Coatings* **2022**, *12*, 669. [CrossRef]
48. Lee, J.; Kim, C.; Liu, C.; Wong, M.; Cápiro, N.; Pennell, K.; Fortner, J. Ultra-high capacity, multifunctional nanoscale sorbents for PFOA and PFOS treatment. *NPJ Clean Water* **2023**, *6*, 62. [CrossRef]
49. Wightman, R.M. Detection Technologies. Probing Cellular Chemistry in Biological Systems with Microelectrodes. *Science* **2006**, *311*, 1570. [CrossRef]
50. Ding, S.; Mosher, C.; Lee, X.Y.; Das, S.R.; Cargill, A.A.; Tang, X.; Chen, B.; McLamore, E.S.; Gomes, C.; Hostetter, J.M.; et al. Rapid and label-free detection of interferon gamma via an electrochemical aptasensor comprising a ternary surface monolayer on a gold interdigitated electrode array. *ACS Sens.* **2017**, *2*, 210. [CrossRef]
51. McEwen, G.D.; Chen, F.; Zhou, A. Immobilization, Hybridization, and Oxidation of Synthetic DNA on Gold Surface: Electron Transfer Investigated by Electrochemistry and Scanning Tunneling Microscopy. *Anal. Chim. Acta* **2009**, *643*, 26. [CrossRef]
52. Jia, Y.; Qian, J.; Pan, B. Dual-functionalized MIL-101 (Cr) for the selective enrichment and ultrasensitive analysis of trace per-and poly-fluoroalkyl substances. *Anal. Chem.* **2021**, *93*, 11116–11122. [CrossRef]
53. Nirschl, M.; PocketVNA, Rohrdorf, Germany. Personal communication, 2024.
54. Q-Sense Explorer Specifications. Available online: https://www.biolinscientific.com/qsense/instrument/qsense-explorer#specifications (accessed on 19 May 2024).
55. Alassi, A.; Benammar, M.; Brett, D. Quartz Crystal Microbalance Electronic Interfacing Systems: A Review. *Sensors* **2017**, *17*, 2799. [CrossRef]
56. Montagut, Y.J.; García, J.V.; Jiménez, Y.; March, C.; Montoya, A.; Arnau, A. Frequency-shift vs. phase-shift characterization of in-liquid quartz crystal microbalance applications. *Rev. Sci. Instrum.* **2011**, *82*, 064702. [CrossRef]
57. Schmitt, R.F.; Allen, J.W.; Wright, R. Rapid design of SAW oscillator electronics for sensor applications. *Sens. Actuators B* **2001**, *76*, 80. [CrossRef]
58. Zou, M.; Dong, M.; Zhao, T. Advances in Metal-Organic Frameworks MIL-101(Cr). *Int. J. Mol. Sci.* **2022**, *23*, 9396. [CrossRef]
59. Radjenovic, J.; Duinslaeger, N.; Avval, S.S.; Chaplin, B.P. Facing the Challenge of Poly- and Perfluoroalkyl Substances in Water: Is Electrochemical Oxidation the Answer? *Environ. Sci. Technol.* **2020**, *54*, 14815. [CrossRef]
60. Tian, Q.; Chen, S.; Shi, M.; Gao, T.; Zhang, M.; Liao, C.; Li, X.; Dong, Q.; Wang, C. Fluorine-functionalized MOF modified GCE for highly sensitive electrochemical detection of persistent pollutant perfluorooctanoic acid. *Sens. Actuators B* **2024**, *404*, 135309. [CrossRef]
61. Dalapati, R.; Hunter, M.; Mostakim, S.K.; Yang, X. Fluorescence Turn-on Detection of Perfluorooctanoic Acid (PFOA) by Perylene Diimide-Based Metal–Organic Framework. *ACS Appl. Mater. Interfaces* **2024**. [CrossRef]
62. Suwannakot, P.; Lisi, F.; Ahmed, E.; Liang, K.; Babarao, R.; Gooding, J.J.; Donald, W.A. Metal–Organic Framework-Enhanced Solid-Phase Microextraction Mass Spectrometry for the Direct and Rapid Detection of Perfluorooctanoic Acid in Environmental Water Samples. *Anal. Chem.* **2020**, *92*, 6900. [CrossRef] [PubMed]
63. Chen, B.; Yang, Z.; Qu, X.; Zheng, S.; Yin, D.; Fu, H. Screening and Discrimination of Perfluoroalkyl Substances in Aqueous Solution Using a Luminescent Metal–Organic Framework Sensor Array. *ACS Appl. Mater. Interfaces* **2021**, *13*, 47706. [CrossRef] [PubMed]

64. Khan, R.; Uygun, Z.O.; Andreescu, D.; Andreescu, S. Sensitive Detection of Perfluoroalkyl Substances Using MXene–AgNP-Based Electrochemical Sensors. *ACS Sens.* **2024**. [CrossRef] [PubMed]
65. Lu, D.; Zhu, D.Z.; Gan, H.; Yao, Z.; Luo, J.; Yu, S.; Kurup, P. An ultra-sensitive molecularly imprinted polymer (MIP) and gold nanostars (AuNS) modified voltammetric sensor for facile detection of perfluorooctance sulfonate (PFOS) in drinking water. *Sens. Actuators B* **2022**, *352*, 131055. [CrossRef]